RADC-TR-75-240
In-House Report
December 1975

A FINE-WIRE MICROTEMPERATURE PROBE FOR ATMOSPHERIC MEASUREMENTS

Darryl P. Greenwood
David B. Youmans

Approved for public release;
distribution unlimited.
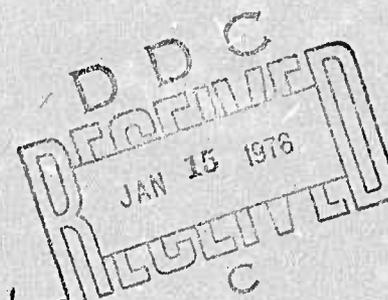
The views and conclusions contained in this document are those of the authors and should not be interpreted as necessarily representing the official policies, either expressed or implied, of the Defense Advanced Research Projects Agency or the U. S. Government.

Rome Air Development Center
Air Force Systems Command
Griffiss Air Force Base, New York 13441

This report has been reviewed by the Office of Information (OI), RADC, and approved for release to the National Technical Information Service (NTIS). At NTIS, it will be available to the general public, including foreign nations.

This report has been reviewed and is approved for publication.

APPROVED: *Vincent J Coyne*
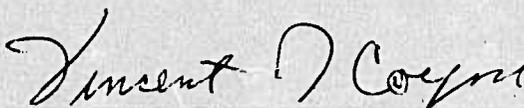
VINCENT J. COYNE
Chief, Space Surveillance and Instrumentation Branch
Surveillance Division

APPROVED: *Rudolf C. Paltauf*
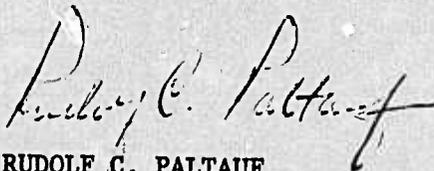
RUDOLF C. PALTAUF
Lt Col, USAF
Chief, Surveillance Division

FOR THE COMMANDER: *John P. Huss*
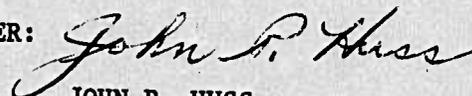
JOHN P. HUSS
Acting Chief, Plans Office

REPORT DOCUMENTATION PAGE		READ INSTRUCTIONS BEFORE COMPLETING FORM
1. REPORT NUMBER RADC-TR-75-240	2. GOVT ACCESSION NO.	3. RECIPIENT'S CATALOG NUMBER
4. TITLE (and Subtitle) A FINE-WIRE MICROTEMPERATURE PROBE FOR ATMOSPHERIC MEASUREMENTS.		5. TYPE OF REPORT & PERIOD COVERED 1 July 1974 - 30 June 1975 In-House Report
		6. PERFORMING ORG. REPORT NUMBER ARPA Order Number 2646
7. AUTHOR(s) Darryl P. Greenwood David B. Youmans		8. CONTRACT OR GRANT NUMBER(s) N/A
9. PERFORMING ORGANIZATION NAME AND ADDRESS Rome Air Development Center (OCSE) Griffiss Air Force Base, New York 13441		10. PROGRAM ELEMENT, PROJECT, TASK AREA & WORK UNIT NUMBERS Program Code Number 5E20 Program Element 62301E Job Order No. 26460107
11. CONTROLLING OFFICE NAME AND ADDRESS Defense Advanced Research Projects Agency 1400 Wilson Blvd Arlington VA 22209		12. REPORT DATE December 1975
		13. NUMBER OF PAGES 58
14. MONITORING AGENCY NAME & ADDRESS(if different from Controlling Office) Rome Air Development Center (OCSE) Griffiss Air Force Base, New York 13441		15. SECURITY CLASS. (of this report) UNCLASSIFIED
		15a. DECLASSIFICATION/DOWNGRADING SCHEDULE N/A

16. DISTRIBUTION STATEMENT (of this Report)

Approved for public release; distribution unlimited.

ARPA Order-2646

17. DISTRIBUTION STATEMENT (of the abstract entered in Block 20, if different from Report)

Same

18. SUPPLEMENTARY NOTES
This research was supported by the Defense Advanced Research Projects Agency of the Department of Defense and was performed by Darryl P. Greenwood and David B. Youmans, RADC (OCSE), Griffiss Air Force Base, New York 13441.

19. KEY WORDS (Continue on reverse side if necessary and identify by block number)
Atmospheric Optics
Microthermal Fluctuations
Propagation
Turbulence

20. ABSTRACT (Continue on reverse side if necessary and identify by block number)
     Refractive-index fluctuations which affect optical propagation depend mostly on microthermal variations. Fine wire probes are sufficient to measure microtemperature so long as we have ready access to the propagation medium. A complete sensor unit currently in use includes the probe, a Wheatstone bridge and amplifier circuit, and a mechanical support assembly. In providing complete details on how to construct such a unit, we concentrated on a design developed in-house which we know to be effective. The unit is found to have a

over

309 050

20.   Abstract (Cont'd)

frequency range better than 0.01 to 100 Hz and responds to minimum temperature
fluctuations of 0.015°C. Of special importance is the low construction cost
of only about $200.

FOREWORD

The work presented in this report is a result of in-house efforts conducted in support of ARPA Orders 2646 (TEAL BLUE II) and 1279 (High Energy Laser Development). The development of the microthermal sensor described here was done at the RADC Advanced Optical Test Facility, Verona Test Site, New York by personnel of the Environmental Studies Section. Some of these sensors have been used at various remote sites such as the ARPA Maui Optical Station in Hawaii and have proven reliable.

The authors wish to thank Mr. Russell McGregor, Mr. Donald Tarazano and Capt. John Bradham for their assistance in data acquisition, processing and interpretation. The assistance through the past few years of Drs. John Wyngaard, J. Chandran Kaimal and Duane Haugen of the AFCRL Boundary Layer Branch in providing direction to the RADC micrometeorology program is especially appreciated.

Most importantly we acknowledge the assistance of Gerald Ochs and Robert Lawrence of the NOAA Wave Propagation Laboratory. A sensor very similar to the one described herein was initially designed and built at NOAA. At this point we may have lost sight of what was developed at RADC and what at NOAA, but in any case we express our sincere gratitude to NOAA for providing the initial guidance necessary for building such a sensor.

i

TABLE OF CONTENTS

LIST OF FIGURES

iii

LIST OF TABLES

I. INTRODUCTION

In studying the effects of the turbulent atmosphere on optical propagation, we must measure the strength and character of the turbulence in order to reference propagation measurements to the current conditions. Without such a measurement of conditions, the propagation results would only be phenomenological, and it would be difficult to extend the measurements to other sites. It is not sufficient to measure gross meteorological parameters such as wind speed, wind direction, humidity, barometric pressure and temperature; although these are important. Rather microtemperature fluctuations are sufficient to describe the turbulence which affects optical propagation.

Refractive-index depends on atmospheric pressure, water vapor and temperature. Pressure fluctuations are of sufficiently low amplitude to be totally ignored. Water vapor, or humidity, fluctuations are significant in the radio wavelengths, but in the optical range their effect over land is typically less than 10%. So we are left with temperature fluctutations, and that is what we measure and relate directly to refractive-index turbulence. Refractive-index is not measured directly, except to the extent that we also propagate optical waves through the atmosphere and record the effect of the rapidly changing refractive-index.

The basic descriptor of temperature turbulence is C_T^2, the temperature fluctuation parameter, which is defined as the

1

constant of proportionality in the inertial-subrange form of the temperature structure function $D_T(r)$, given by the Kolmogorov form

$$D_T(r) = \langle (T_1 - T_2)^2 \rangle$$
$$= C_T^2 r^{2/3}, \quad \ell_0 << r << L_0, \tag{1}$$

where T_1 and T_2 = temperatures at positions 1 and 2 with separation r, ℓ_0 = inner scale and L_0 = outer scale. Notice that C_T^2 is not defined from measurements of D_T where r is outside the range indicated; and moreover if the exponent of r is not 2/3, then the turbulence is not Kolmogorov and C_T^2 is not defined at all. We shall consider an instrument which will give us measures of C_T^2 as well as functions such as $D_T(r)$ and the temperature fluctuation temporal power spectrum $F_T(f)$.

Our basic requirements on the probe are that it be sufficiently short to resolve small scale fluctuations, and that it be of sufficiently small diameter to be able to respond rapidly enough to the highest frequency fluctuations. Also the sensor circuitry must respond to very low frequencies to account for fluctuations of size larger than the outer scale. Typically the inner scale is a few millimeters and the outer scale is on the order of height above ground. We can use these scales to designate a desired frequency range of $v/(2\pi L_0)$ to $v/(2\pi \ell_0)$ where v = wind speed. If we suppose v ranges from 1 to 5 m/sec, ℓ_0 = 6 mm, and L_0 = 10 m, then the nominal frequency range is

10^{-2} to 10^2 Hz. Our design will have a somewhat better frequency range.

The particular sensor, with its associated circuitry, is described in the next section. An overall view of the unit is provided as Fig. 1. In general the probe, which is a short, extremely thin platinum wire, is mounted as one leg of a Wheatstone bridge circuit. The resistance of the probe is very nearly proportional to temperature; and thus temperature changes are sensed as an imbalance voltage of the bridge. This imbalance voltage is amplified so that the overall sensor has a response in the order of 0.5 v/°K.

We shall follow the sensor description of the next section with instructions on how to manufacture probes, an outline of the steps employed in field use and detailed instructions on how to manufacture a complete microthermal sensor unit. Then we will conclude with a description of the data processing procedures used in the current operation.
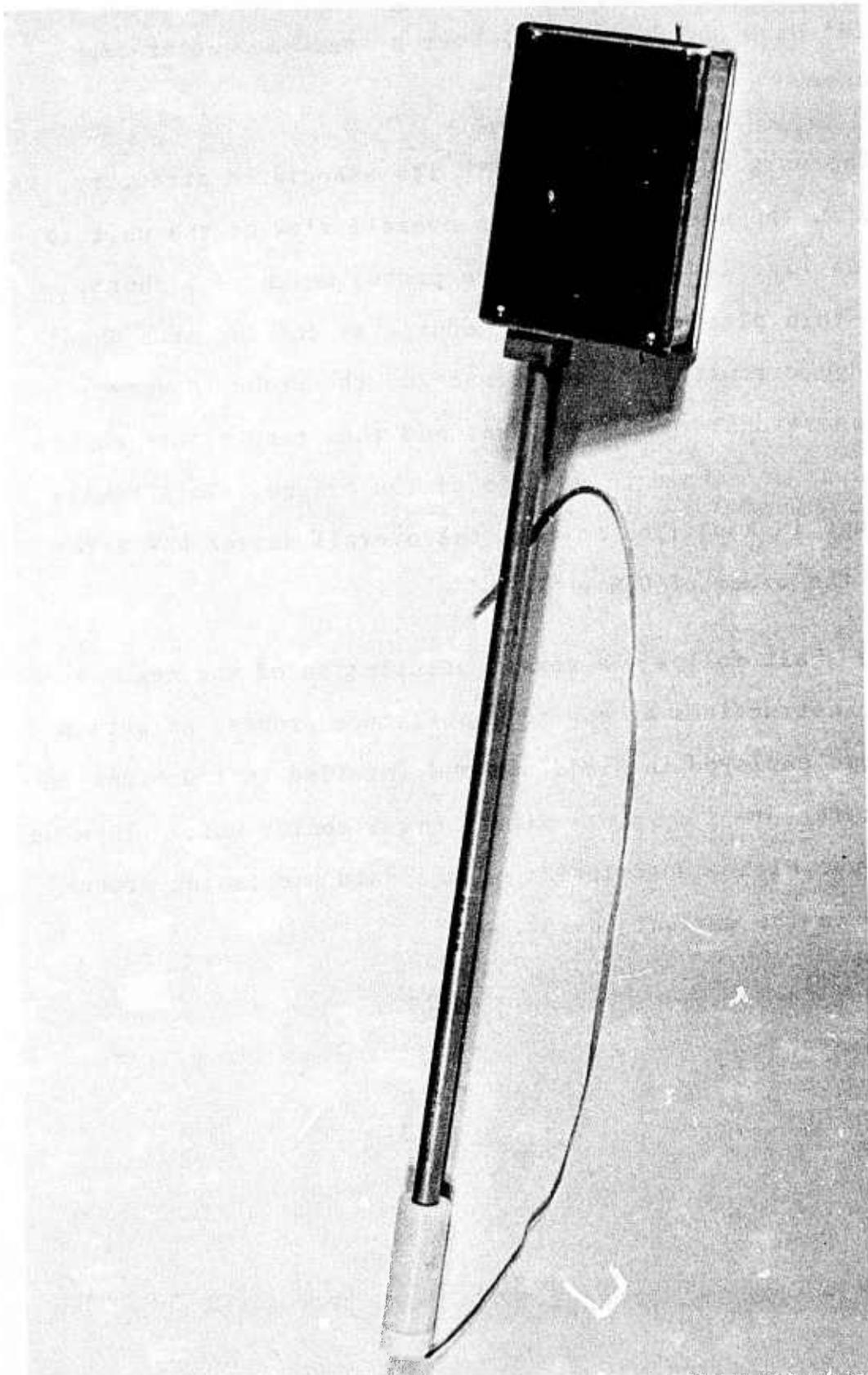
Figure 1. Overall photographic view of Microthermal Sensor
Unit. Length overall approx. 25 1/2 inches.

4

II. SYSTEM DESCRIPTION

A. The Probe Itself.

The microthermal probe is a piece of Wollaston-process silver-on-platinum wire which has been etched so as to remove the silver. The remaining platinum acts as the active element. The Wollaston process allows the drawing of extremely thin wires by inserting a platinum core inside a much larger tube of silver. The silver is of a diameter 100 times larger than the core. The composite is drawn in a conventional manner and both materials are reduced in diameter. The resultant wire is roughly 250 μm in diameter, with a platinum core of about 2.5 μm. A short section (about 1 to 1.5 cm in length) of the wire is soldered at its ends to a pair of posts. Then about a 2 mm length of the wire is immersed in nitric acid to remove the silver. The resultant resistance of the exposed platinum is about 20 Ω/mm. For a photograph of the probe, refer to Fig. 2.

Platinum has a very nearly linear temperature-resistance characteristic curve, with a constant of proportionality of about 0.00393 Ω/°K. More precisely we can describe this curve with the Calender-van Dusen equation[1]:

$$\frac{R_s(T)}{R_s(0)} = 1 + \alpha[T + \delta(1 - T/100)(T/100) + \beta(1 - T/100)(T/100)^3] \quad (2)$$

where $R_s(T)$ = sensor resistance at temperature T in °C, and for pure, annealed, strain-free platinum wire we have:
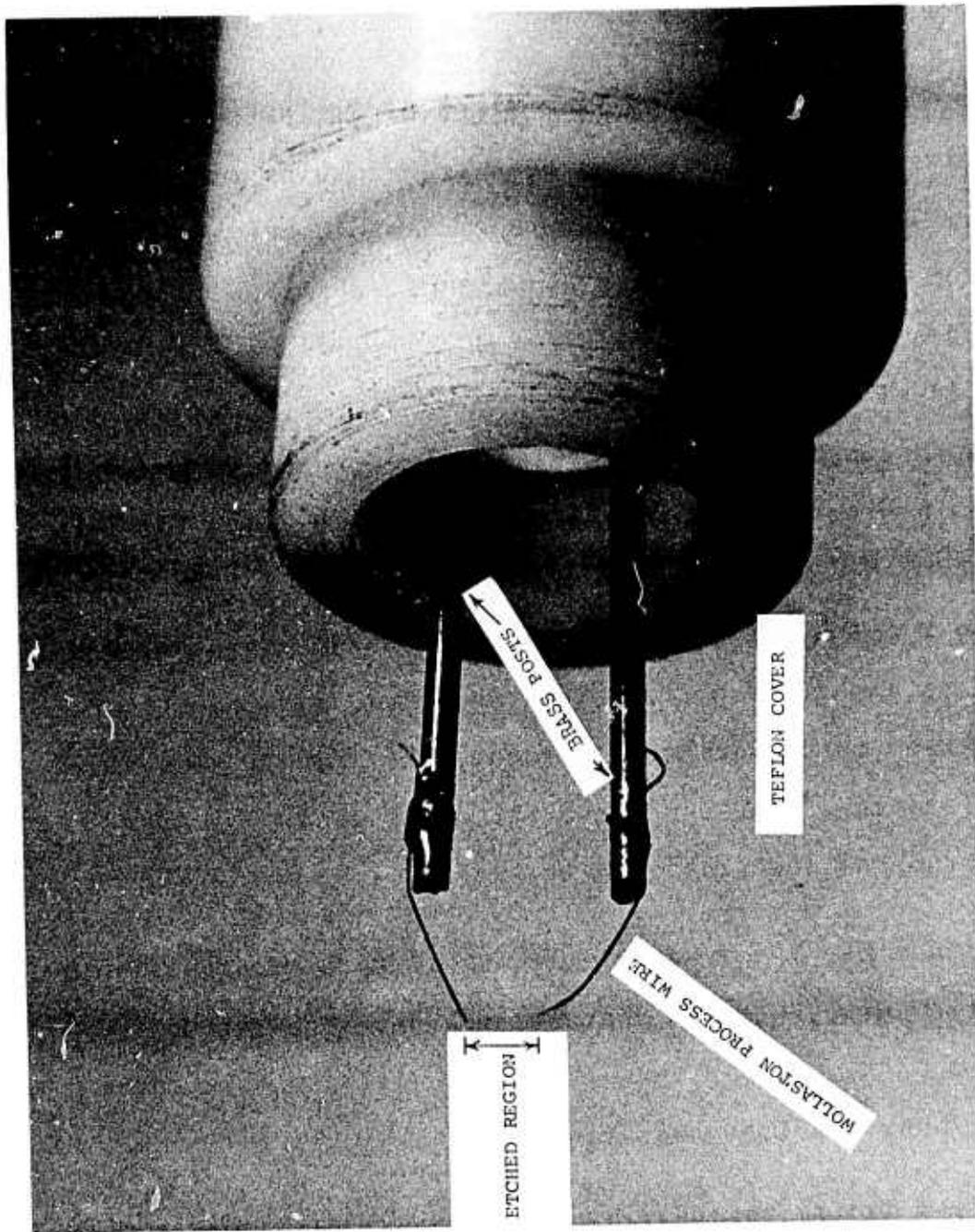
Figure 2. Photographic view of probe end of Microthermal Sensor. Cap has been removed and protective sleeve pulled back to put probe in its normal operating configuration.

6

$\alpha = 0.00393\ \Omega/°K$

$\delta = 1.49$

and $\beta = 0.110$ for $T < 0$ and $\beta = 0.00$ for $T > 0$.

For convenience, values of Eq. (2) for the temperature range of interest are given in Table 1.

Ochs[2] uses sensors which are 0.6 µm in diameter, and they have a response time of about 200 µsec in still air or about 70-80 µsec in winds of 2 to 5 m/sec. Measurements of the response time of a 2.5 µm wire were made by Ochs[3] as 900 µsec in still air and 300 µsec in winds of about 5 m/sec. Wyngaard[4] corroborates these values with measurements of the response time of a sensor used in the RADC experiments, finding about 800 µsec in still air. The values are for "dirty" sensors, ones which have been used for a day or so. "Clean" sensors, freshly made, may have response times at least one-half the aforementioned values. By response time we mean the time it takes the output voltage of the bridge to go 63.2% of its final value after the sensor sees a step change in temperature. Since the response is exponential, the sensor acts as its own low pass filter with a power response of $[1 + (2\pi f T)^2]^{-1}$ where T is the response time.

B. The Circuit.

The sensor is mounted as one leg of a Wheatstone bridge shown in Fig. 3 and is indicated by $R_s(T)$. The balance potentiometer R_p is adjusted so that the output voltage E_{out} is

7

Table 1. $R_s(T)/R_s(0)$ versus temperature $T(°C)$ for typical pure, annealed, strain-free platinum resistance temperature sensor.   From Rosemount.[1]

T(°C)	$R_s(T)/R_s(0)$
0	1.0000000
1	1.0039830
2	1.0079648
3	1.0119455
4	1.0159251
5	1.0199035
6	1.0238807
7	1.0278568
8	1.0318316
9	1.0358053
10	1.0397778
11	1.0437492
12	1.0477193
13	1.0516882
14	1.0556561
15	1.0596228
16	1.0635883
17	1.0675527
18	1.0715157
19	1.0754777
20	1.0794385
21	1.0833982
22	1.0873567
23	1.0913139
24	1.0952699
25	1.0992249
26	1.1031787
27	1.1071313
28	1.1110828
29	1.1150330
30	1.1189821

To convert a measured value of R_s at T to R_s at 0°C, divide $R_s(T)$ by the appropriate number above.

nearly zero. (This is done when the switch is in the DC position.) The imbalance voltage due to temperature fluctuations is amplified by a series of two operational amplifiers shown in Fig. 3. The circuit is sufficiently straightforward, so we will not go into its details. Later, under construction details, we will provide photographs as well as printed circuit board layouts of the circuit.

For the bias voltage and resistance values given in Table 2, and applying to Fig. 3, we find that the current drawn by the probe is about 450 µa. According to tests made by Ochs[2], this implies we have a cold-wire probe as long as the wind velocity exceeds about 0.5 m/sec. In fact we recommend that the reader peruse that report for significant supplemental information.

The sensor amplifier has a pair of capacitors each labeled C_2 between first and second stages to allow AC coupling of the stages. The values used provide a 100 sec time constant, and thus the -3 dB point of the high pass single pole filter is at 1.6×10^{-3} Hz. This is sufficiently low to encompass scale sizes larger than most values of L_0 and for typical winds. As long as the circuit is enclosed in a nearly-airtight container and the components have low drift, there will not be a significant low frequency drift problem.

A relatively straightforward analysis of the circuit in Fig. 3 gives us this gain equation:
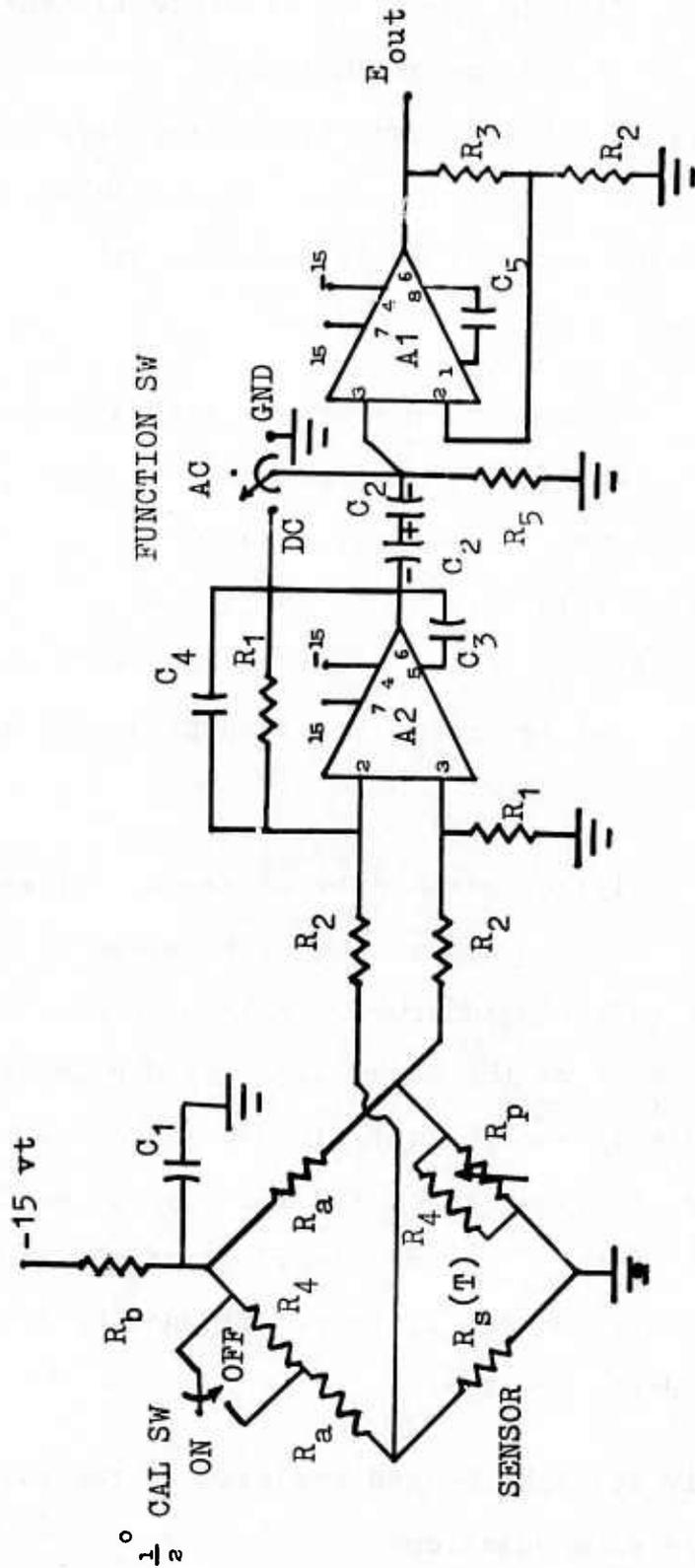
Figure 3. Circuit diagram for Bridge/Amplifier. Component values in Table 2.

10

Table 2. Component list for Bridge/Amplifier

Code	Quantity	Value	Item
A1	1	-	Analog Devices AD208H Op. Amp.
A2	1	-	Analog Devices AD504LH 7235H Op. Amp.
C1	1	500 μfd	15 WVDC Mallory MTV500 DW15 Capacitor
C2	2	200 μfd	25WVDC Sprague TE-1213, Capacitor 30 D207G025DH2
C3	1	390 μμfd	±5% Elmenco Mica 7FA391G031 Capacitor
C4	1	220 μμfd	±5% Elmenco Mica 7FC221G03 Capacitor
C5	1	10 μμfd	±5% Elmenco Mica 6CD100K03 Capacitor
Ra	2	30.1 KΩ	±1% IRC Resistor T055 (MIL RN55D)
Rb	1	2.74 KΩ	±1% IRC Resistor T055
R1	2	500 KΩ	±1% IRC Resistor T060 (MIL RN60D)
R2	3	1 KΩ	±1% IRC Resistor T055
R3	1	10 KΩ	±1% IRC Resistor T055
R4	2	100 Ω	±1% IRC Resistor T055
R5	1	1 MΩ	±1% IRC Resistor T060
Rp	1	200 Ω	Amphenol Potentiometer 994SL201
-	2	-	Amphenol Connector 7 Pin #197 (Panel Plug)
-	2	-	IC Socket Cinch - Jones 8-ICS
$R_s(T)$	1 spool	-	Wire 0.1 mil diameter platinum, silver coated, 5747 Ω/Ft at 20°C, #408, Sigmund Cohn Corp., Mt. Vernon, NY
FN SW	1	-	Subminiature Switch, Switchcraft JMT-121
CAL SW	1	-	Subminiature Switch, Switchcraft JMT-123
Cable	as req'd	-	Alpha #3241 (2 conductor w/shield)
Cable	as req'd	-	Alpha #3242 (3 conductor w/shield)
-	as req'd	-	Amphenol Connector 7 Pin #195 (Cable to Panel Plug)
-	1	-	Power Supply Zeltex ZM1550

$$\frac{E_{out}(T)}{T-T_1} = \frac{E \ G \ R_s(0)}{2R_b + R_a} \ \alpha \ (1 + \delta/100) \tag{3}$$

where T_1 = Temperature (°C) when bridge is nulled

   E = Bridge bias voltage (-15 v)

   R_b = Bias resistance (2.74 KΩ)

   R_a = Resistance in two legs of the bridge (30.1 KΩ)

and G = Voltage gain of the amplifier (-5500).

(In evaluating Eq. (3), we approximated Eq. (2) to within 1% for the temperature range of 0 to 30°C.) After substitution of the component values into Eq. (3) we find

$$\frac{E_{out}(T)}{T-T_1} = \frac{R_s(0)}{108.2} \tag{4}$$

where $R_s(0)$ is in ohms and $E_{out}(T)/(T-T_1)$ is in v/°C. Hence a sensor resistance of 54.1 Ω will yield a 0.5 v/°C gain of the system. (A one volt per °C gain could be achieved with a value of $R_s(0)$ = 54.1 Ω by changing R_1 to 1 MΩ.) To convert an actual output voltage to temperature changes, multiply E_{out} by $108.2/R_s(0)$.

Note that the above two equations have $R_s(0)$ as an element. Normally R_s is measured at some temperature other than 0°C. So it is convenient that soon after measurement of R_s, it be converted to $R_s(0)$ either by using the Calender-van Dusen equation, Eq. (2) or the numbers in Table 1.

12

The maximum operating range of the circuit is ± 10v; so for a gain of 0.5 v/°C, the range of temperature excursions is ± 20°C. The ambient operating point can drift by only that amount when the function switch is in the DC position. However, when AC operation is used, the operating point may drift around in the range ± 200°C. This assumes that the drift is of frequencies below the 1.6×10^{-3} Hz high-pass filter cutoff. Thus AC operation allows the sensor to be run untended for long periods of time. It also allows the user to keep the temperature fluctuations around 0 v, which is optimum for the recording and subsequent digitization and processing.

C. Operational Testing.

The sensor units may be operationally tested in two ways. (We will assume that a well-calibrated probe, perhaps from a commercial concern, is not available as a reference.) Both approaches involve recording output data and processing the signals for power spectral densities. The processing scheme used is outlined in section V. The first test is for the entire unit, with the exception of the probe wire itself. The probe is carefully immersed in oil, so that minimum temperature fluctuations are sensed. The unit is operated normally otherwise. This gives us a measure of the noise level. Second, we operate a series of probes in the atmosphere under normal operating conditions. Their outputs are recorded and compared with theory and each other.

13

The oil bath test consists of submersing just the probe in approximately 2 qt. of #10 weight oil and allowing the temperature of the oil to stabilize to ambient temperature. With the exception of the probe being in the oil, care should be taken to have all other operating conditions as nearly normal as possible. That is, the sun should be shining on the unit, and the wind velocity should be at a reasonable value. For an additional reference, a second probe should be operated normally in the atmosphere within a few meters of the sensor being tested. Once confidence has been developed in constructing the units, this step of an oil-bath test can be skipped. An example of such spectra is given in Fig. 4. Total mission time was 60 min and $C_T^2 = 0.113$ °C^2 $m^{-2/3}$. Note that this value of turbulence is high, and there is a two decade separation between the two spectra shown. There are two regions of the oil spectrum to note. The lowest frequency power, below 0.5 Hz is still dominated by drift of the oil bath; hence an f^{-2} power law. The remainder of the power is the composite noise of the bridge, amplifier, coaxial cable, tape recorder amplifiers and analog tape. The conclusion is that for reasonably high values of C_T^2, say above 10^{-3} °C^2 $m^{-2/3}$, the noise is not a significant problem. If we include the drift region of this oil spectrum, the equivalent noise level is found from an integral of the spectrum to be 0.016°C (rms); however if we ignore the drift, the noise level is 0.015°C (rms). The latter figure is consistent with the value of 0.02°C reported by Lawrence et al.[5]

14
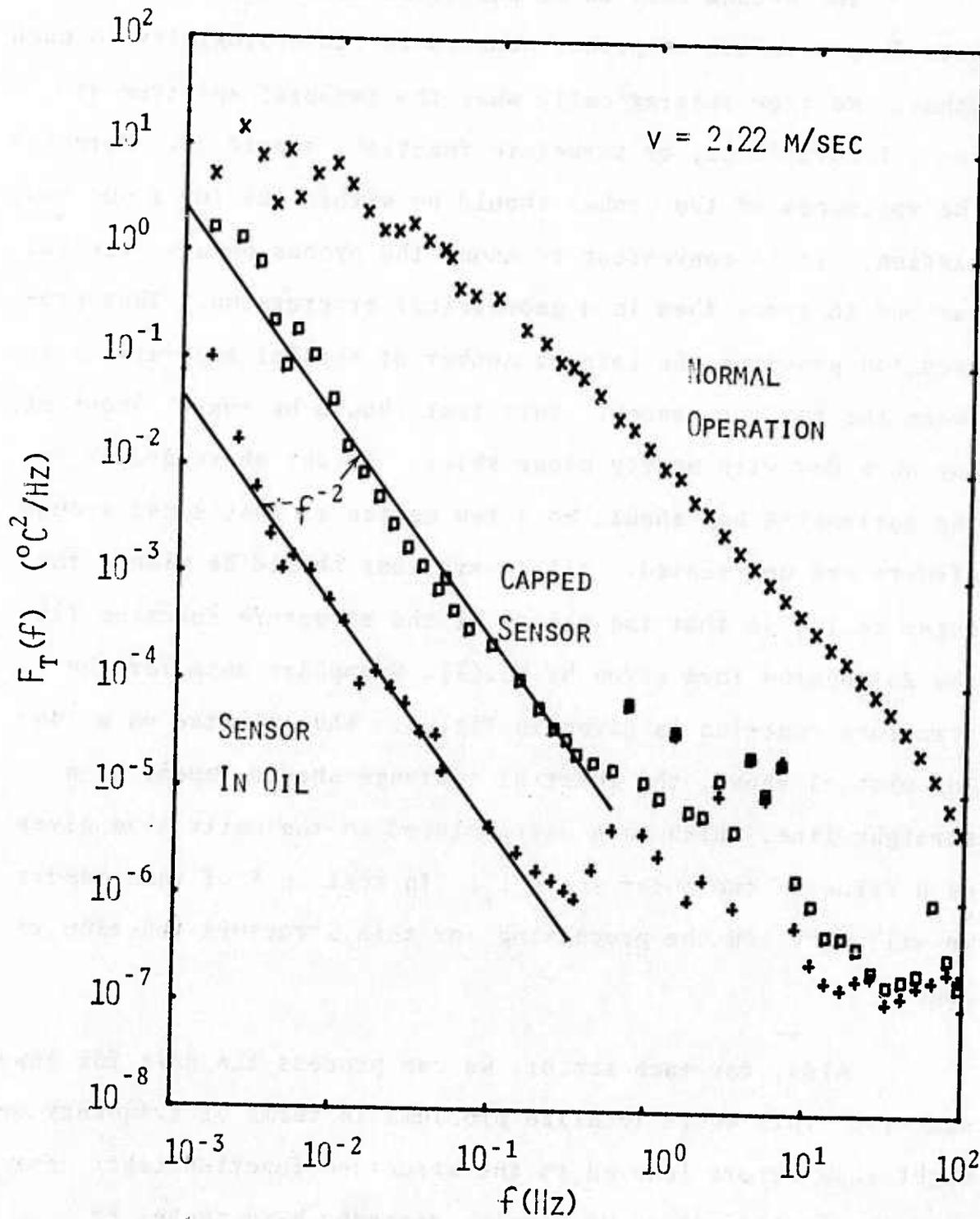
Figure 4.   Temperature power spectra for a sensor in oil, a sensor in air and a sensor with its teflon cap in place.

15

The second test to be performed is to look at the outputs from a series of probes mounted in close proximity to each other. We know theoretically what the temporal spectrum and spatial covariance, or structure function, should be. Moreover the variances of the probes should be within 10% for a one hour mission. It is convenient to mount the probes on a horizontal bar and to space them in a geometrical progression. That progression provides the largest number of spatial separations between the various probes. This test should be run at about midday on a day with mostly clear skies. Height above ground for the horizontal bar should be a few meters so that local ground effects are not sensed. All separations should be within the outer scale, so that the values of the structure function fit the Kolmogorov form given by Eq.(1). Exemplary data for the structure function is given in Fig. 5. When plotted on a log-log plot as shown, the inertial subrange should appear as a straight line, which when extrapolated to the unity line gives us a value of the outer scale L_0. In section V of this report we will show how the processing for this structure function is done.

Also, for each sensor, we can process the data for power spectra. This would localize problems in terms of frequency and might show errors ignored in the structure function test. For example significant 60 Hz ripple, recorder head noise, or amplifier drift might be isolated. In the inertial subrange, basically between $v/(2\pi L_0)$ and $v/(2\pi \ell_0)$, the spectrum should

16
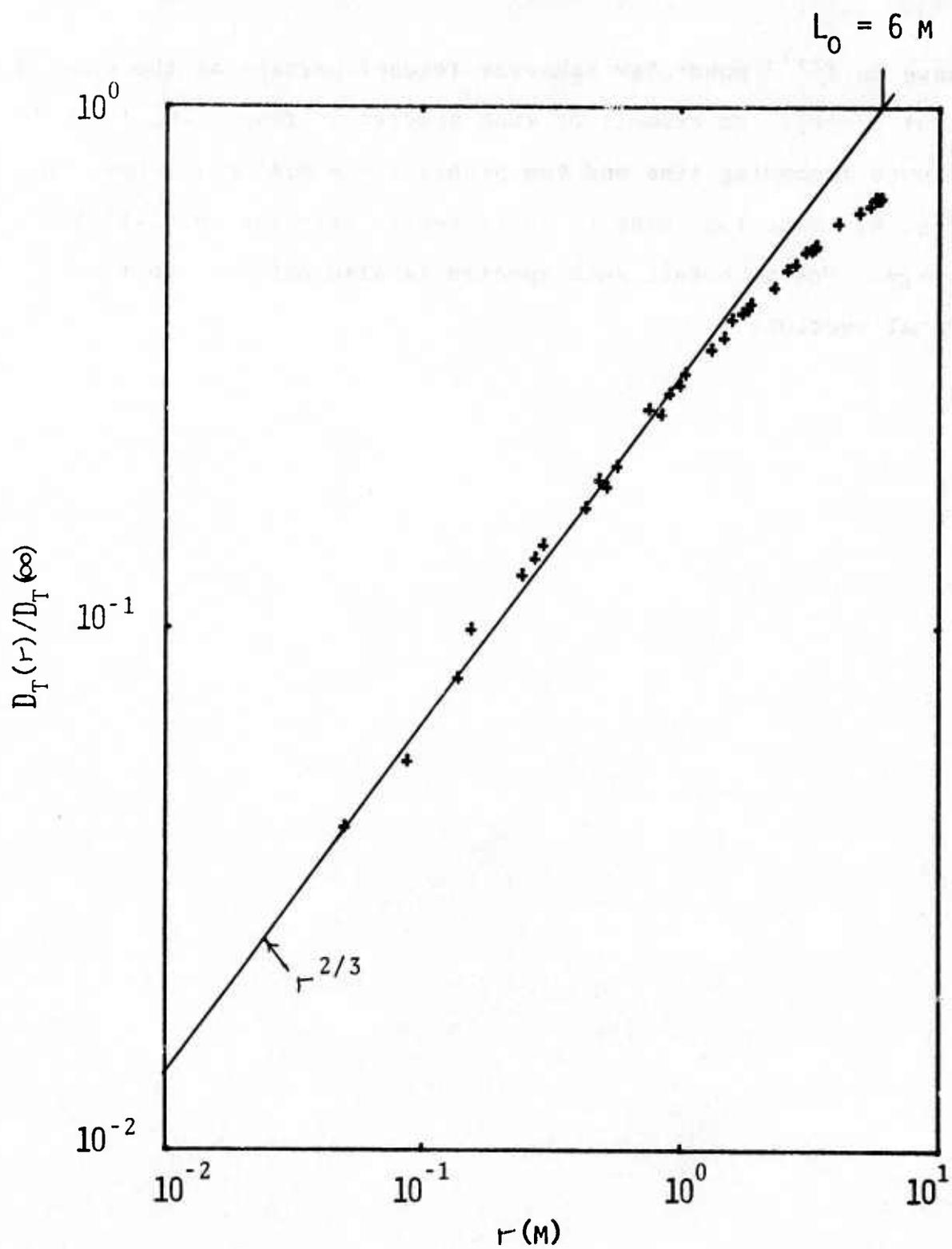
Figure 5.   Normalized temperature structure function data
collected 1 Oct 73 at Verona test site, Griffiss AFB
NY.   Outer scale L_0 indicated as intersection of the
extrapolation of the inertial subrange with the unity
line.

17

have an $f^{-5/3}$ power law behavior (except perhaps at the ends of that range). An example of such spectra corresponding to a 150 minute recording time and two probes space 0.43 m is shown in Fig. 6. Note the curve is quite smooth over the inertial sub-range. How we obtain such spectra is also outlined in the final section.
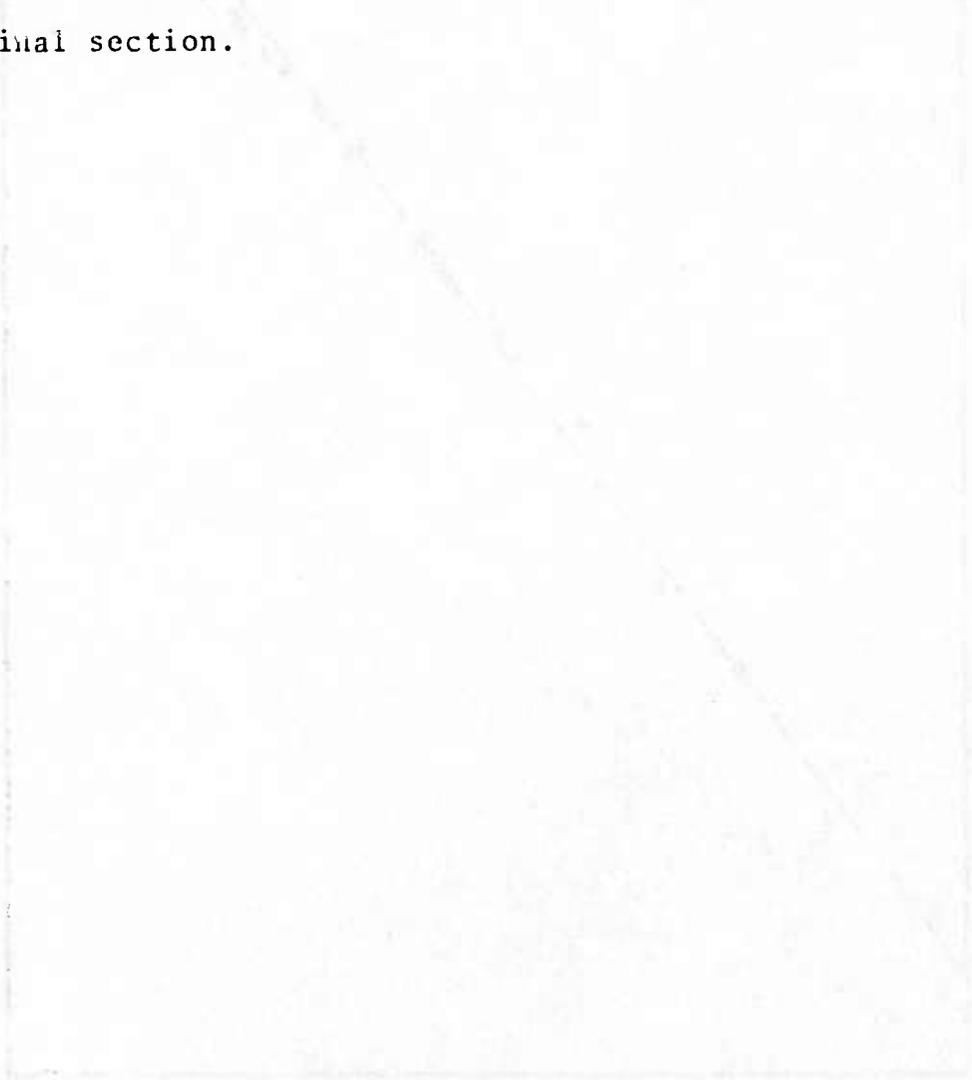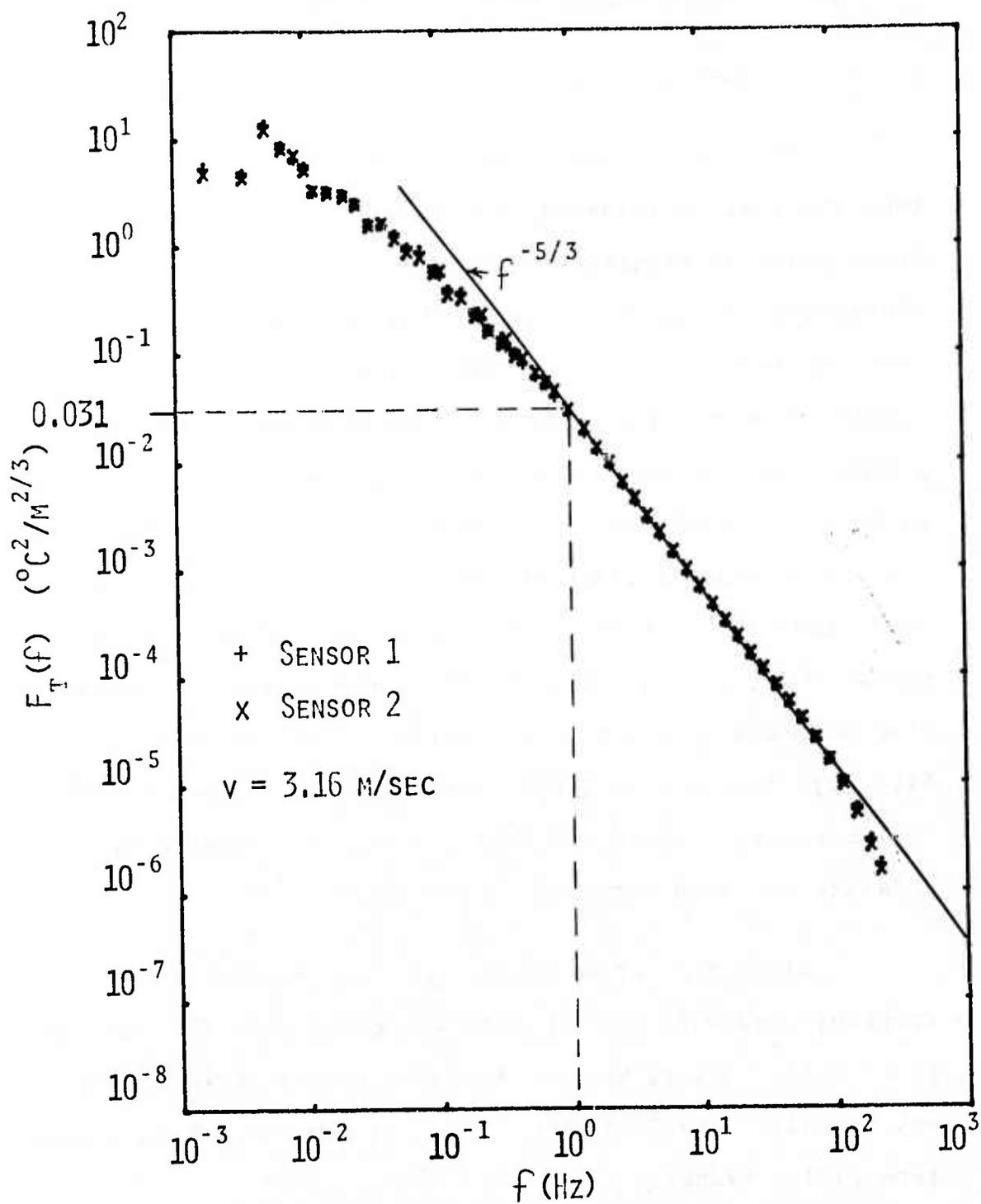
Figure 6. Temperature power spectral density data for same mission as Fig. 5. Two probes were operated simultaneously. Inertial subrange indicated as an $f^{-5/3}$ power law.

19

III. SENSOR PROBE REPAIR, CALIBRATION AND OPERATION

A. Manufacture of Sensor Probes.

The fabrication of the Wollaston wire probe requires that the wire be soldered to a pair of sturdy binding posts of brass prior to etching with nitric acid. (Refer again to the photograph of Fig. 2.) The binding posts are themselves soldered securely to a two wire cable with aluminum shield. The shield is soldered only to the printed circuit card chassis ground strap to minimize 60 Hz ground loops. Earlier sensor units were fabricated with a probe plug-socket arrangement. However an investigation of Calender-van Dusen equation, Eq. (2), shows that only a 0.004 Ω rms change in the apparent sensor resistance due to variations in the probe-socket resistance will give an additional 0.02°C rms noise. (This assumes $R_s(0) = 54.1 \Omega$.) Indeed even larger variations in the probe-socket resistance were noted and this approach was abandoned. This emphasizes the need for good solder connections.

At this point we assume that the binding posts are available and will describe how to mount, etch and test the probe wire. Later, we will describe the construction of the entire unit. The following steps are recommended for manufacture of the probes:

1. Prepare the nitric acid for etching in this manner:

    a. Obtain a 40% solution of reagent grade HNO_3.

    b. Use an eye dropper to produce a controlled drop of acid.

20

c. Clamp the eye dropper vertically on a vertical post stand.

d. Attach a small screw type clamp to the rubber bulb of the eye dropper. The size of the acid drop is controlled by the adjustment of the clamp.

2. Solder the unetched wire in place by these steps:

a. Use a 40 watt soldering iron.

b. Clean the probe binding post of any residual solder and place a small amount of solder on each post.

c. Place one end of the Wollaston wire against one binding post and heat the post without touching the wire.

d. Bend the wire over to the other post while forming a loop of about 10 to 15 mm in length.

e. Hold the free end of the wire against this post with a small piece of tape.

f. Solder the wire to the binding post without touching the wire with the soldering iron, and remove the tape.

g. Test the solder connection of the loop mechanically by inserting a small ¼ inch diameter rod (the shank of a drill bit) inside the loop and pushing lightly outward.

3. Etch the wire in this manner. (Insure that the DC supply voltage is not connected to the unit at this point.)

a. Clamp the probe support rod to a second vertical stand in such a way that the wire can be inserted into the nitric acid.

b. Attach a very low current ohmmeter across the output

wires of the probe, preferably making the connections

at the printed circuit card. (An HP 3440A with plug

in 3444A is an adequate ohmmeter.)

c. Record the resistance value which may be as high as

0.4 Ω.

d. Place about 2 mm of the tip of the wire loop in the

suspended drop of nitric acid by lowering the eye drop-

per. At normal room temperature it will take about ten

minutes for the probe resistance to reach approximately

58 Ω. At lower temperatures (say 10°C), etching may be

extremely slow, and an auxiliary heater may be needed to

raise the ambient temperature to about 20 to 25°C.

e. Remove the probe wire when the resistance is approxi-

mately 58 Ω (± 5 Ω typically). Note that a 2 mm length

of 20 Ω/mm wire would give us 40 Ω resistance; so we are

certain that the silver is removed if we go beyond 40 Ω.

f. Remove the probe support rod from its clamp and momen-

tarily submerge the wire loop in a breaker containing a

saturable solution of baking soda in tap water. This

neutralizes any residual acid.

4. Complete the calibration of the sensor with these steps:

a. Record the probe resistance and the ambient temperature

in the vicinity of the probe.

b. Subtract the initial resistance value as found in step

3. c. from the resistance found in step 4. a.

c. Use Table 1 or the Calender-van Dusen equation to

determine $R_s(0)$ given $R_s(T)$, where T was the ambient temperature at time of measurement.

d. Record the sensor identification number and the value of $R_s(0)$. It is this value of $R_s(0)$ that should be kept with the unit until the sensor breaks; $R_s(T)$ is not of value any longer and may confuse those using the data.

e. Connect the DC supply leads to the unit, set the function switch to ground then to the DC position, and adjust the bridge balance pot R_p so that the output voltage E_{out} is nearly zero ($\pm$ 0.05 v). A slight imbalance here will not affect the final output, as we will operate in an AC coupled mode.

f. Measure and record the rms voltage output (with the probe covered). This value should not exceed 2 mv.

B. Field Operation.

For optimum turbulence response, the sensor should be oriented so that there are no obstructions upstream of the probe. If the wind direction is fairly steady (10°rms), this means that the rod on which the probe is mounted be pointed into the wind. If the wind direction fluctuates considerably, then the probe support rod should be mounted vertically to have proper exposure for all wind directions.

If an array of probes is used, so as to develop a spatial correlation or structure function, then the line of probes should be normal to the wind direction. Then there will be no

23

wake effects from one sensor to the next. Generally the data will still be acceptable as long as the wind direction does not come within 25° of the line connecting the probes for more than 10% of the time. The operator should be prepared for large fluctuations in wind direction, and if the mean shifts radically, he should reposition the bar.

The distance downwind from an obstacle such as a building should be at least 100 times the size of the obstacle. This includes concrete or asphalt roads or parking lots as well. Of course, there may be times when the user wishes to know turbulence levels in the vicinity of such obstacles and this rule will not apply. Good quality microtemperature data will be collected, however, when well-developed turbulence conditions exist. Typically this means mostly clear skies, daytime conditions and wind speeds exceeding 1 m/sec.

The sensor power supply requirements are + 15 v and - 15 v at ± 3 ma maximum. The supply may be a commercial rectifier with filtering or may be a battery. The maximum length of the power cable should be 100 ft. The power cable is of #18 wire, including 2 twisted leads and a ground shield lead. Power supplies may be located near the sensors, so this length requirement is not a real restriction. The sensor unit signal cable should also be two wires plus a ground shield. Normal load to the sensor is 10 KΩ. A signal cable of #18 wire, one mile in length, is less than 100 Ω in resistance. Hence the signal cable

length can be quite long without having a serious degradation, provided the sensor unit load is 10 KΩ or higher.

The steps in placing the sensor unit into operation are as follows:

1. Place the power supply switch to ON.

2. Keep the probe sensor covered.

3. Place the function switch in the DC position.

4. Adjust the sensor unit output voltage to near zero (±0.05 v) while adjusting the bridge pot R_p. The ability to actually set this voltage to near zero depends upon the quality of R_p.

5. Lightly tap the sensor unit chassis and observe the output voltage. Any changes occurring in the output voltage are probably a result of a poor solder connection which must be repaired.

6. Record the output voltage.

7. Place the ½ degree calibration switch to ON. The output voltage should change by .4 ± .05 v for a 58 Ω probe resistance. (It would be proportionally more or less for a higher or lower R_s, respectively.)

8. Uncover the probe.

9. Gently blow on the probe and observe the positive voltage excursions which occur. This insures the unit is sensing temperature variations of some sort.

10. Place the function switch in the GND position, and then to AC. This will remove any residual charge on the C_2 pair and will prepare the circuit for AC operation.

11. Observe the sensor voltage output on a chart recorder.

Make sure there is no voltage saturation occurring in the ± 10 v operational range.

12.   The sensor unit now operational.   The probe should not be uncovered in winds over 12 m/sec or in conditions of dust or precipitation, as they will break easily.   In fact, any sort of jar to the system might break or stretch the probe.

IV. CONSTRUCTION

In previous sections we considered that the operational units are available to the user and thus we only covered set-up, calibration and routine usage. Now we will describe how the circuit, enclosure and probe support are manufactured, especially emphasizing rationale for certain design schemes. In retrospect we feel this is not necessarily a compact design, as since these units were first built, more compact integrated circuitry has been made available.

A. The Circuit.

Fabrication of the high gain sensor unit requires good engineering practice in order to reduce microphonics, component value drift, rf noise pick-up, 60 Hz pick-up and corrosion. Microphonics have been eliminated by using a printed circuit board and strong solder connections. Noise pick-up from external rf sources is greatly reduced by mounting the printed circuit card inside an enclosed aluminum chassis, and by mechanically attaching the probe support tube to the chassis. By enclosing the circuitry in the aluminum box, no air currents are present which could induce temperature variation in the components and thus component value drift. Corrosion of components and solder joints is eliminated by using weather sealed covers on the aluminum chassis.

The 60 Hz pick-up is reduced to less than the amplifier

27

background noise output level by using two independent ground connections. The two systems are not connected at any point but at the recording system so as to minimize ground loops. (To better understand the following, refer to Fig. 7 of the printed circuit card.) The first ground is a connection of the shield of the output signal cable to the GROUND BUSS on the printed circuit card. This in turn is connected to the aluminum chassis and the shield for the cable leading to the microthermal probe. As with the signal cable, a two-twisted-wire cable with shield is used for the probe. The power supply cable is however three-wire with a shield, but this shield is connected at the power supply end of the cable directly to the power supply case. None of the wires from the power supply is connected to the aforementioned GROUND BUSS. The second ground system is a connection of the "low" sides of the probe and output signal two-wire leads to the COMMON GROUND. The power supply zero-voltage lead is also connected to the COMMON GROUND. Thus to avoid a ground loop from the power supply, this lead must be floated at the power supply.

The gain of the sensor unit must have a high order of stability over a range of ambient temperatures from -30°C to 40°C. Therefore all resistors are metal film, of ± 1% tolerance and have a temperature coefficient of ± 100 PPM/°C from -55°C to 175°C.

The printed circuit board layout of Fig. 7 is

FIG. 7A.   OBVERSE VIEW
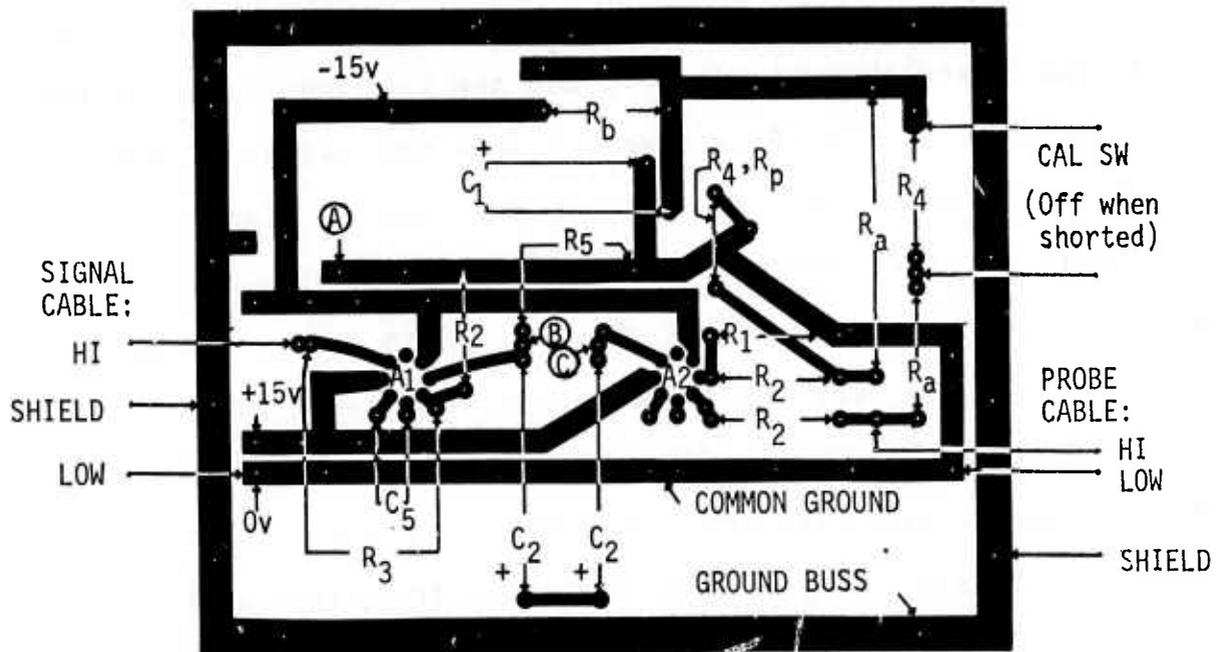
FIG. 7B.   REVERSE VIEW, WHERE THE PRINTED CIRCUIT IS ETCHED.
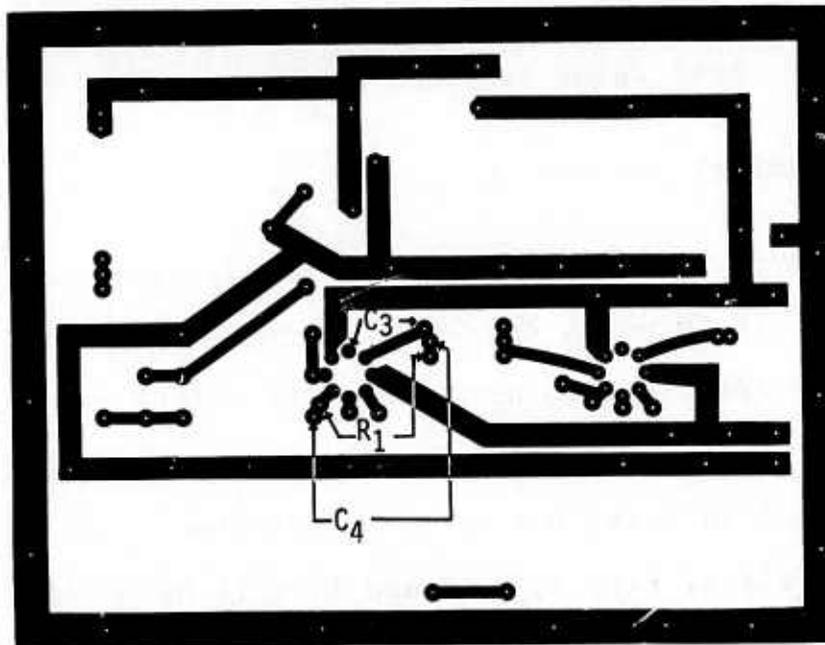
Figure 7.   Layout of printed circuit board.   Symbols A, B and C
denote the connection points for the function switch.
(Connecting A to B implies GND, B to C implies DC, and
no connection for AC.   See Fig. 9.)

supplemented with an exact 1:1 scale layout of the mask used in photo-etching, Fig. 8. Note that the printed circuit is underneath the board shown in Fig. 7, and the components are on top. Thus the mask in Fig. 8 is reversed from the layout of Fig. 7. In Figures 9 and 10 are the obverse and reverse side views of the board after components have been mounted, and after the board has been secured to the chassis. Note that components C_3, C_4, C_5 and R_1 are mounted directly to the operational amplifier sockets. Five small additional capacitors show up in Figs. 9 and 10 and were added just prior to the time the photograph was taken. They are not listed in the parts list of Table 2 and are not shown in Fig. 7. They were used to reduce exceptionally high rf pick-up in one experiment and connect from the GROUND BUSS to ± 15 v, 0 v, and to the two leads of the probe cable. Their value is 0.002 µfd (50 WVDC).

B. The Mechanical Support Assembly.

We have provided full engineering drawings of the sensor unit in Figs. 11-18 which should be sufficient for the construction of units identical to ours. Certain points may be improved upon; however our intent is to provide plans for a working system and not present anything not tried in practice. The various photographic views, Fig. 1, 2, 9 and 10 will be helpful in following this discussion. In Table 3 we have listed those parts for which government stock numbers exist. Note that this list does not cover all parts needed, as we anticipate that the

30
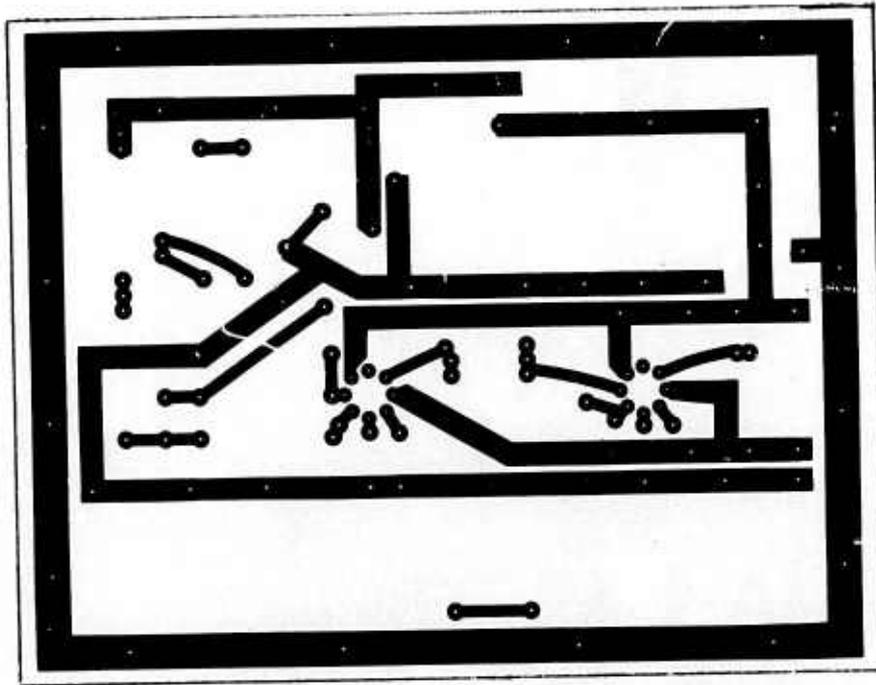
Figure 8. Photograph of mask used in photo-etching of printed circuit board. Exact 1:1 scale used in printing.

CROSS SLIDE SCREW

PROBE SUPPORT TUBE

PROBE CABLE

CAL SWITCH

ON

OFF

SIGNAL CABLE PLUG

POWER CABLE PLUG

DC
AC
GND

FUNCTION SWITCH
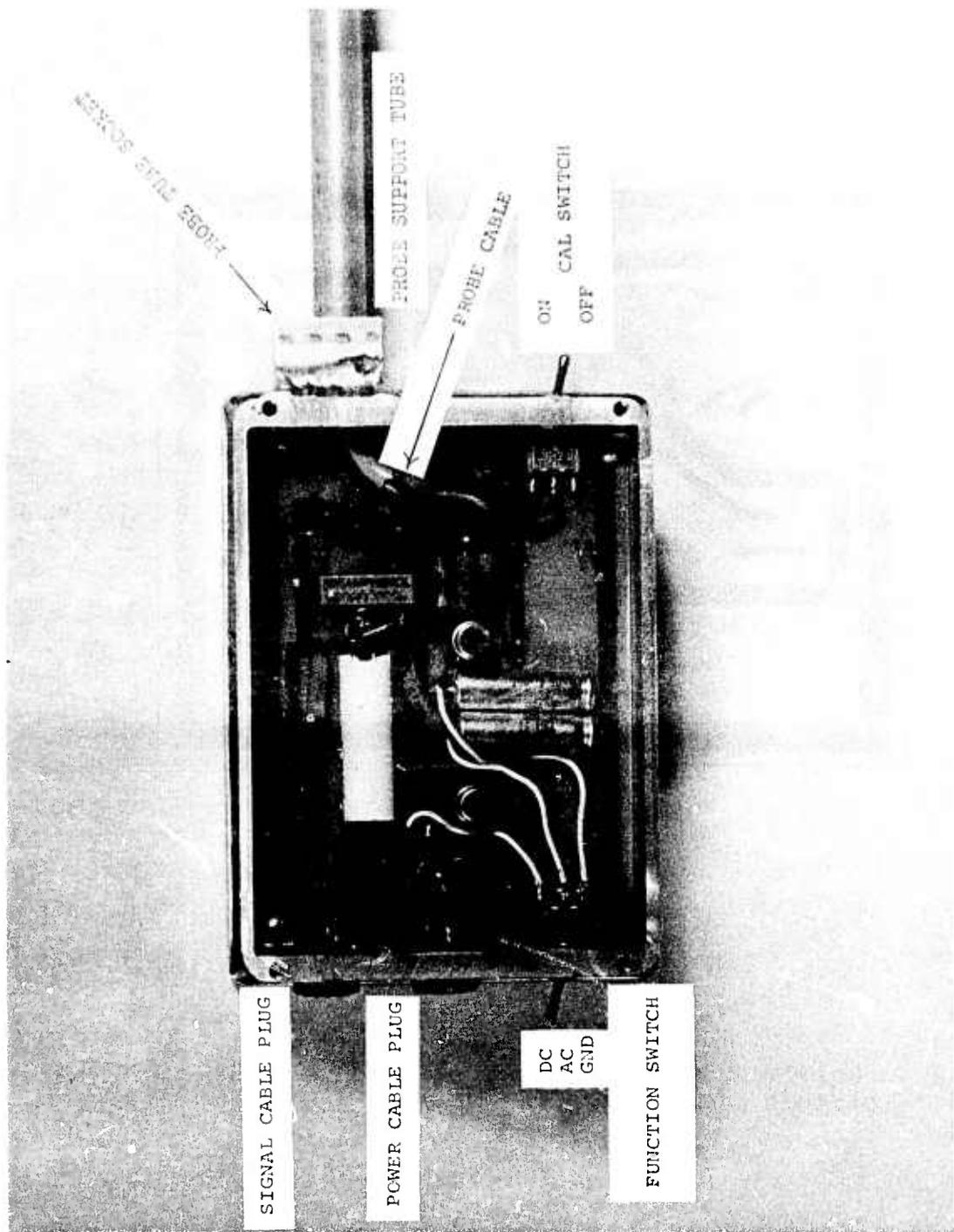
Figure 9. Obverse side photographic view of printed circuit, components and chassis.
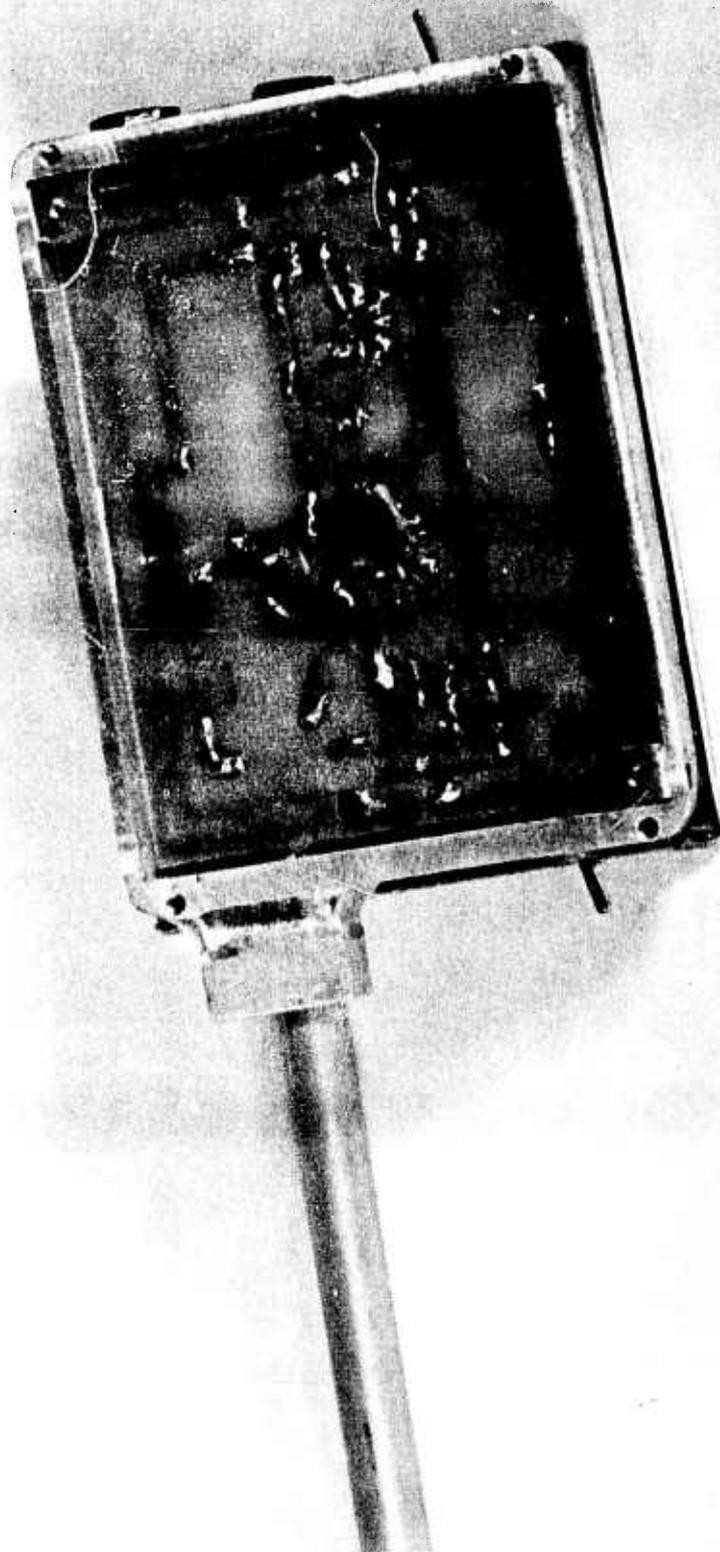
Figure 10.   Reverse side photographic view of printed circuit, components and chassis. The circuit itself is etched on this side.

Figures 11-18. Engineering drawings of sensor unit, including

   11. Overall layout

   12. Chassis

   13. Covers for chassis

   14. Cap to cover probe

   15. Sleeve to cover probe

   16. Rods for mounting probe

   17. Holder for rods of Fig. 16

   18. Sensor support tube

NOTES: REMOVE ALL SHARP EDGES

BREAK LIP APPROX. AS SHOWN (4 SIDES) MIN. RADIUS

GASKET MATL: MED. RUBBER JOG THE CEMENT TO COVER

.250 (TYPICAL)

.31

3.61

3.18

.12

5.00

5.25

.18

45°

BREAK LINE

.149 DIA. 4 HOLES

REVISIONS

ZONE | LTR | DESCRIPTION | DATE | APPROVED

U.S. AIR FORCE
RADC-GAFB, N.Y.

LIST OF MATERIALS

Stan Yerger

TITLE

Cover - Housing

ALUM. 5052-H32

UNLESS OTHERWISE SPECIFIED
DIMENSIONS ARE IN INCHES
TOLERANCES ON

FRACTIONS ± 1/64
.XX ± .01
.XXX ± .005

ANGLES ± 1/2°

SIZE | FSCM NO. | DWG NO.
C | 07877 | X7518754

SCALE FULL

ENGINEERING DRAWING LAYOUT C

7518756

APPLICATION

QTY REQ'D

REVISIONS

LTR	DESCRIPTION	DATE	APPROVED

CHAMFER
.02 ±.05°

.060 DIA.

.12

.50

.748 DIA. +.002 −.000

1.00

MATL : NYLON

7518756

NEXT ASSEMBLY   USED ON

APPLICATION

AF FORM 1653 AUG 72   PREVIOUS EDITION WILL BE USED.

REVISIONS

LTR	DESCRIPTION	DATE	APPROVED

TAP #6-32 NC

.25

.38

3.00

.750 DIA. +.000 -.002

1.00

.505 DIA. +.002 -.000

PARTS LIST

MATERIAL / SPECIFICATION

U.S. AIR FORCE
RADC - GAFB, N.Y.

SLEEVE

MATL: NYLON

07877

X7518752

SIZE B

SCALE FULL

ENGINEERING DRAWING LAYOUT B

APPLICATION

7518756

NEXT ASSEMBLY

QUANTITY REQUIRED PER DASH NO.

AF FORM 1853 PREVIOUS EDITION WILL BE USED.

FLATTEN END
APPROX. AS SHOWN

.040 DIA.

.023 DIA.

2.00

.25

.02

REVISIONS

ZONE	LTR	DESCRIPTION	DATE	APPROVED

U.S. AIR FORCE
RADC-GAFB, N.Y.

TIP - SENSOR

X7518751

.040 DIA.
BRASS

7518756

APPLICATION

ENGINEERING DRAWING LAYOUT B

AF FORM 1653
SEP 63

40

Holder-Tip — Drawing No. X7518750

.113 DIA.
.06 DEEP

.480 DIA.

.12

.50

.18

NYLON

.400 DIA.

.039 DIA.
2-HOLES

.25

REVISIONS
ZONE	LTR	DESCRIPTION	DATE	APPROVED

U.S. AIR FORCE
RADC-GAFB, N.Y.

HOLDER-TIP

07877   X7518750

B

SHEET 2 of 1

NYLON

7518756		1	1
NEXT ASSY	USED ON	NEXT ASSY	FINAL ASSY
			QTY REQD
APPLICATION			

41

42

Table 3. List of materials for constructing sensor unit,
         excluding electronics.

1. Aluminum tubing - Stock #4710-278-6411, 1/2 inch outside
    diameter, wall thickness 0.05 inch, weldable 6061.

2. Aluminum bar - Stock #9530-247-5514, 1/8 inch thick, 2 inch
    wide, weldable 6061.

3. Aluminum bar - Stock #9530-237-0721, 1/4 inch thick, 1 1/4
    inch wide, weldable 6061.

4. Aluminum bar - Stock #9530-244-9026, 3/4 inch thick, 3/4
    inch wide, weldable 6061. (Alternative: aluminum tubing
    3/4 inch OD, 1/8 inch wall thickness.)

5. Aluminum sheet - Stock #9535-232-6868, 0.063 inch thick,
    weldable 5052.

6. Rubatex Insulation Tape - 1/8 inch thick by 2 inch wide
    (Rubatex Corp., Bedford VA).

7. Teflon (or Nylon) cylindrical bar - 1 inch diameter

8. Teflon (or Nylon) cylindrical bar - 1/2 inch diameter

machinist will have common materials, such as screws, nuts, etc., in stock.

Rather than discuss each of the eight engineering drawings in detail, we will break the unit into three general parts: chassis (Figs. 12, 13), probe cover (Figs. 14, 15) and probe support tube (Figs. 16-18). The overall unit is assembled in Fig. 11.

The chassis is fabricated from weldable aluminum 6061. Chassis sides (long dimension) are from 1/8 inch by 2 inch bar stock and the ends are from 1/4 inch by 1 1/4 inch bar stock. The chassis corners are secured by welding. The two chassis covers are fabricated from aluminum flat sheet 0.06 inch thick. Edges have been bent down for a better appearance and to avoid sharp edges. Along the inner edges of the covers, where the covers mate to the chassis sides, strips of rubber have been used so that air currents may not enter the box. The probe tube socket (labeled in Fig. 9) may be made from 3/4 inch by 3/4 inch bar stock, and is welded to the chassis. An alternative material, shown in Fig. 12, is stock tubing, 0.75 inch outside diameter, 0.5^+ inch inside diameter. The probe tube socket is drilled and tapped on two sides for #20 set screws which secure the tube. The tube could be welded in place if the user never expected to interchange longer or shorter tubes, and this would prevent moisture from entering the chassis at this point. The tube and socket could be threaded, as well. The

44

printed circuit card is fastened to the inside of the chassis
by means of two cubical aluminum holders which are tapped for
6/32 inch screws. The holders are secured to the inner walls
of the chassis by welding, as shown. We suggest preparing tem-
plates for use in drilling the holes into the chassis for the
mounting of switches and sockets, and for the holes for the
chassis cover plates.

The probe support tube (indicated in Fig. 9 and drawn in
Fig. 18) is also from weldable aluminum stock 6061, 0.5 inch
outside diameter with a wall thickness of 0.049 inch. At the
probe end of the tube, a slot is milled longitudinally (along
the rod) beginning at a point 1/2 inch from the end of the tube
and extending for 2 1/4 inches. The groove is 1/8 inch wide and
0.03 inch deep. In addition a 1/2 inch long slot, 1/8 inch in
width and 0.03 inch deep is milled laterally from the end of the
longitudinal slot at the end of the tube nearest the probe.
This groove provides a track for the set screw in the teflon
cover, when the cover is brought forward to cover the probe.
The lateral slot allows the cover to be rotated about 90° after
it is slid over the probe. The sensor end of the probe support
tube is fitted with a teflon cylinder to hold the two brass rods
which in turn support the Wollaston process wire. (This cylinder
is not shown in the photographs but is detailed in Fig. 17.)
The cylinder is of diameter 0.4 inch and is 1/2 inch in length.
To secure the cylinder, a #4 set screw is inserted through the
side of the tube. The rods are two inches long and 75 mil in

45

diameter (re Fig. 16). The teflon cylinder is drilled for the insertion of the rods at the spacing shown in Fig. 17. Once the rods are in place, the probe cables may be soldered to the rods and the cylinder inserted into the tube. The material used for the rods is a brass-alloy welding rod.

The probe cover is fabricated from 1 inch outside diameter solid teflon or nylon rod. The three inch long section of teflon rod shown in Fig. 15 is drilled for smooth insertion of the 1/2 inch diameter tube. The rod is cut back 0.38 inch of its length to an outside diameter of 3/4 inch. A 1 inch diameter by 1/2 inch long cap (in Fig. 14) is then machined to fit over the 3/4 inch diameter end of the teflon rod. The opposite end of the rod is tapped for a #6 thumb screw. This screw permits the probe to be covered by sliding the teflon cover over the end of the sensor and attaching the cap. The cap is fitted with a long string, as shown in Fig. 1, so that the cap may be held in place.

V. DATA PROCESSING SYSTEM

A. The Recording Scheme.

The purpose of the data processing system is to provide temporal and spatial statistical information on the turbulent temperature of the atmosphere. In addition to the microtemperature measurements, common meteorological observables which are recorded include wind speed, wind direction, barometric pressure and the gross temperature from a dew-point system. Nine microthermal probes are oriented in a geometrical progression on a horizontal boom positionable two to eight meters above the ground. This makes a total of thirteen signals which are recorded digitally on a narrow bandwidth system and on analog tape for subsequent wide bandwidth processing. The digital unit is the Analog-Digital Data System model 100M Data Logger, with a 12 bit analog-to-digital converter. The sample rate is 400 Hz divided by the number of channels currently in use. For the 13 channels, the rate is about 31 Hz. This narrow bandwidth system is used for obtaining those statistical quantities which are not sensitive to aliasing: especially probability densities, variances, spatial cross-covariances and higher order moments. For spectral information on the turbulence, all thirteen signals are recorded in parallel on analog tape. The Ampex FR1200 tape recorder has at 3 3/4 ips a bandwidth of DC to 1250 Hz (-3 dB) and the tapes used have bandwidths superior to that. Later two

channels at a time are converted from analog-to-digital on a 12-bit PDP-8 computer. Because the possibility of aliasing will be significant to the subsequent Fourier analysis, a low-pass filter is inserted in each channel prior to conversion. The -3 dB point of the Krohn-Hite model 3322 filters is set to the Nyquist frequency, one-half the sample rate, and the roll-off is that of a four-pole Butterworth filter, -80 dB/decade. Sample rates from 200 to 700 Hz are chosen depending on the expected noise level.

B. Digital Processing.

The digital tapes from the ADDS unit and from the PDP-8 are processed in two separate software packages on a Honeywell 635/645 computer. One program computes the cross-covariance matrix of the thirteen signals by operating on the tapes from the ADDS unit. Matrices are generated for averaging times typically ranging from 10 to 30 minutes. The microtemperature elements of the matrix are then converted into a plot of $1-C(r)$ where $C(r)$ is the spatial correlation. Such a plot is identical to $D_T(r)/D_T(\infty)$, where, once again, D_T is the structure function. In the end an average $1-C(r)$ plot is generated for the entire mission. This program also calculates C_T^2 according to its definition Eq. (1) and calculates L_0 as the separation r where the extrapolated inertial subrange of $1-C(r)$ intersects the unity line. An example of such data is given in Fig. 5.

The second program operates on the tapes from the PDP-8

48

computer and provides wide bandwidth power spectral densities. For a full description of this program we direct the reader to Jayne and Foley[6]. The six spectra are the individual spectra of the two temperatures, the difference spectrum, the modulus and phase of the cross-spectrum and the coherency. The signals are first transformed via a fast discrete Fourier algorithm for frequencies from $f_{ny}/2048$ to f_{ny}, where f_{ny} is the Nyquist frequency. Namely 4096 data points per channel are transformed at one time. The data are then digitally low-pass filtered by a four-pole Butterworth with a cut-off of $f_{ny}/64$. The low-frequency part of the spectrum is then obtained by transforming the remaining signal which has been decimated, keeping only one point in sixty-four. The low and high frequency spectra undergo constant percentage bandwidth averaging so that on a logarithmic frequency scale, the spectral estimates appear to have a nearly constant separation. Sixty-four frequency spectra are averaged to correspond, in averaging time, to a single low-frequency spectrum. Finally, several such spectra are averaged to represent an entire mission. The final averaging time can be computed as $N \cdot 2048 \cdot 64/f_{ny}$, where N is the number of spectra averaged together. Since varying numbers of spectral estimates are averaged to give a final value, the confidence limits are a function of frequency as well as N. Following Blackman and Tukey[7], we assume the spectral estimates follow a chi-squared distribution. Tables in Blackman and Tukey or in Abramowitz and Stegun[8] can be used to generate upper and lower confidence limits. The

49

confidence limits for our spectra never exceeded twice the value at the high side or 1/2 the value at the low side and the error bar size decreased rapidly with increasing frequency.

C. Pertinent Equations.

We now assume that power spectral densities and covariances have been computed and will demonstrate the important parameters which describe turbulence. Most important of these parameters are the temperature structure parameter C_T^2 and the outer scale L_0. We will show how to insure the nature of the turbulence is Kolmogorov and how to treat C_T^2 and L_0 if it is not.

There would be no need to measure both the temporal spectra and the spatial covariance if the assumption of frozen flow were valid. Frozen-flow assumes that we can convert spatial lags into temporal simply by considering the wind velocity as a scale factor. If the turbulence does not change significantly while it is transported through the spatial lags of interest, then the frozen flow assumption is valid. Panofsky, Cramer and Rao[9] state the hypothesis is valid close to the ground for lag distances up to 90 m provided $\sigma_v/v \lesssim 1/3$, where σ_v^2 is the wind speed variance. This translates to equivalency of temporal and spatial spectra for temporal frequencies $f \lesssim v/570$.

So why would we measure both the spatial covariance and the temporal power spectra? First of all, we are not guaranteed

50

frozen flow behavior. Secondly, we can not obtain an accurate measure of outer scale from the spectra. Thirdly, to obtain a value of C_T^2 from the spectra requires knowledge of wind velocity; whereas it can be derived early from the covariance of two probes with only the knowledge of their separation. We usually use only two probes and calculate their spectra and a single point on the structure function.

Let us first examine the structure function. We compute the covariance matrix

$$C_{ij} = \langle (T_i - \langle T_i \rangle)(T_j - \langle T_j \rangle) \rangle \tag{5}$$

for an array of probes numbered i (or j) = 1, N. The on-axis components are the variances

$$\sigma_i^2 = C_{ii}. \tag{6}$$

For the structure function we return to Eq. (1), repeated here for convenience:

$$D_T(r_{ij}) = \langle (T_i - T_j)^2 \rangle, \tag{7}$$

where r_{ij} is the separation of the two sensors at i and j. If we expand this equation and substitute Eqs. (5) and (6) we find

$$D_T(r) = \sigma_i^2 + \sigma_j^2 - 2C_{ij} + (\mu_i - \mu_j)^2, \tag{8}$$

where $\mu_i = \langle T_i \rangle$.

Without any loss in generality we can assume $\mu_i = \mu_j$. In practice the mean values may be offset only by the electronics, as long

51

as the two probes are at the same height above ground. Thus

$$D_T(r_{ij}) = \sigma_i^2 + \sigma_j^2 - 2C_{ij}. \tag{9}$$

We are now in a position to get values of C_T^2, as long as $r_{ij} << L_0$ (by typically a factor of 10). In a moment we will see how to obtain L_0. So from Eq. (1) we have as many measures of C_T^2 as we have r_{ij}:

$$C_T^2 = D_T(r_{ij}) r_{ij}^{-2/3}, \qquad r_{ij} << L_0. \tag{10}$$

We do not have to concern ourselves with r_{ij} being so small as to provide a measure of the inner scale, since sensors should not be placed within a few millimeters of each other: each would interfere with the flow seen by the other.

If the sampling is of sufficient duration (at least 60 minutes) and the probe units are accurately calibrated with respect to each other, then

$$\sigma_i^2 = \sigma_j^2. \tag{11}$$

(In addition the probes must be at the same height above ground.) Next, we assume that $C_{ij}(\infty)=0$, which is true for all physical processes. Then if we divide $D_T(r_{ij})$ by $D_T(\infty)$ we obtain

$$D_T(r_{ij})/D_T(\infty) = 1 - \rho_{ij} \tag{12}$$

where ρ_{ij} is the cross-correlation coefficient of the two sensors. It is the function $1-\rho_{ij}$ which is plotted in Fig. 5 and

52

which provides us with the outer scale. By definition[†] the outer scale L_0 is the separation r at the intersection of an extrapolation of the $r^{2/3}$ region and the $1-\rho_{ij}$ = unity line. This is indicated in Fig. 5, and there we found L_0 = 6 m for probes 2.2 m above ground level. In order to obtain the number of separations shown in Fig. 5, we oriented nine probes in a geometrical progression. If we have m probes in such a progression, then we have $\sum_{i=1}^{n-1} (n-i)$ independent separations.

The other piece of information we can obtain is whether the turbulence is Kolmogorov or not. The power law dependency in the inertial subrange must be $r^{2/3}$. Our rule of thumb is that the least squares power law should be well within 10% of 2/3 for recording times of at least one hour. Also, we only consider separations $r \lesssim L_0/10$ in making this judgement. The values of $1-\rho_{ij}$ for small r_{ij} have less confidence than those of larger r_{ij}. The reason is that if we assume a fixed percentage confidence limit on ρ_{ij}, then as $\rho_{ij} \to 1$, the values of $1-\rho_{ij}$ become less trustworthy. If we determine that the nature of the turbulence is non-Kolmogorov, we do not throw out our value of L_0. It still represents an "external-scale size." However C_T^2 would be recomputed for a different structure function power law r^p and would be given a new symbol C_T^{*2}. The relation for C_T^{*2} is

---

[†]The outer scale used here is equal to the one obtained from the von Karman spectrum if you multiply the von Karman L_0 by 1.071.

then

$$C_T^{*2} = D_T(r)r^{-p}, \qquad r \ll L_0^*, \tag{13}$$

where L_0^* is the new external scale size. Note that if only two probes are used and the outer scale is sufficiently large, then it is convenient to set $r = 1$ m in advance.

The power spectra also demonstrate whether the turbulence is Kolmogorov. Assuming frozen flow and the form of the structure function given in Eq. (1), we find the spectrum in the inertial subrange to be

$$F_T(f) = 0.0730v^{2/3}f^{-5/3}C_T^2 \tag{14}$$

for $\left[\dfrac{v}{2\pi L_0}\right]^2 \ll f^2 \ll \left[\dfrac{v}{2\pi \ell_0}\right]^2$, where v = wind speed. Note that we now have another way of measuring C_T^2 and it is from a single probe. However we now have the added requirement of measuring wind speed. For convenience we rewrite Eq. (14):

$$C_T^2 = 13.69 \ f^{5/3}v^{-2/3}F_T(f) \tag{15}$$

Values of outer scale could be obtained from spectra but it requires recording times typically much longer than periods of stationarity of the turbulence. It is much more convenient to use a pair of probes at a fixed separation and measure their correlation coefficient. An example of obtaining C_T^2 from spectra is shown in Fig. 6. The inertial subrange power law dependence $f^{-5/3}$ is shown, and from a value of F_T at $f=1$ Hz and $v=3.2$ m/sec we find $C_T^2 = 0.20 \ ^\circ C^2 m^{-2/3}$.

54

The power spectra can be used to give measures of inner scale ℓ_0. However the sensors used must be significantly shorter than ℓ_0, so as not to effect a spatial average. Furthermore, the sensor must respond well in frequencies around $v/(2\pi\ell_0)$ which may be a few hundred Hz. This may require a very fine wire sensor of diameter 0.6 µm. Our sensors respond linearly to approximately 100 Hz, are of diameter 2.5 µm and are 2 mm in length. Hence they are not quite suitable for measuring ℓ_0. The only reason we do not use finer, shorter probe wires is that they are difficult to construct and break easily.

The quantity of interest in the propagation calculations is C_n^2, the refractive-index structure parameter. Once we make the assumption that water vapor and pressure fluctuations are insignificant, we find that C_n^2 is proportional to C_T^2 via

$$C_n^2 = (79.2 \times 10^{-6} p/T^2)^2 \ C_T^2 \tag{16}$$

where p is the ambient pressure in millibars and T is the ambient temperature in degrees Kelvin. The constant 79.2×10^{-6} is correct only at $\lambda = 0.5$ µm, in the middle of the visible range. Tatarskii[10] also reports these values for the constant: 82.9×10^{-6} at $\lambda = 0.3$ µm and 77.4×10^{-6} at $\lambda = 0.7$ µm. We have performed a least squares fit to these three values of the constant and found the relation

$$(72.3503 + 0.6067k - 0.004912k^2) \times 10^{-6} \tag{17}$$

where $k = 2\pi/\lambda$ and λ = wavelength (μm^{-1}) *in the visible range*. We suppose the relation is not too far off in the infrared but have no values to compare with in that range.

55

VI. CONCLUSIONS

We have presented the details necessary to constructing
and using a probe for measuring microtemperature fluctuations
in the atmosphere. The design is for an inexpensive unit which
may cost only about $200 as compared with commerical ones at
least ten times that. Our circuit has no automatic compensation
should the level of fluctuations change radically, and there is
no automatic gain circuit which would compensate for low fre-
quency drifts. The unit is expected to be tended to the extent
that it is to work at near ground level and may be covered in
case of precipitation.

Also we have included no internal processing of the
signal. The data is raw temperature fluctuations, which is pre-
ferred in the type of processing we do. Should the user decide
to redesign the unit, he should keep in mind the major design
criteria outlined throughout the text. We expect that with more
up-to-date circuitry, the entire bridge-amplifier arrangement
might be placed in a volume the size of the teflon probe cover.
If we were marketing this device, that is what we might have
done. However, we have reported on a reliable instrument which
has served us for six years, and we did not change anything in
the design just for the purpose of this report.

REFERENCES

[1] Rosemount Engineering Company, Minneapolis MN, Bulletin 1341 (Rev B), Sept. 1965.

[2] G. R. Ochs, *A Resistance Thermometer for Measurement of Rapid Air Temperature Fluctuations*, ESSA Technical Report IER 47-ITSA 46 (US Dept of Commerce, Washington DC, Oct 1967).

[3] G. R. Ochs, National Oceanic and Atmospheric Administration, Boulder CO, private communication, Nov 1973.

[4] J. Wyngaard, Air Force Cambridge Research Laboratory, Hanscom Field MA, private communication, Nov 1973.

[5] R. S. Lawrence, G. R. Ochs and S. F. Clifford, *J. Opt. Soc. Am.* **60**, 826 (1970).

[6] R. A. Jayne and D. H. Foley, *Data Processing Support to Laser Propagation Program*, RADC-TR-74-284 (Avail NTIS, Washington DC, Oct 1974).

[7] R. B. Blackman and J. W. Tukey, *The Measurement of Power Spectra* (Dover, New York, 1958).

[8] M. Abramowitz and I. A. Stegun, *Handbook of Mathematical Functions* (US Dept of Commerce Applied Mathematic Series 55, Washington DC, 1968).

[9] H. A. Panofsky, H. E. Cramer and V. R. K. Rao, *Quart. J. Roy. Meteorol. Soc.* **84**, 270 (1958).

[10] V. I. Tatarskii, *The Effects of the Turbulent Atmosphere on Wave Propagation* (Israel Program for Scientific Translations, Jerusalem, 1971, Available from US Dept of Commerce, TT68-50464), p. 102.

MISSION
of
Rome Air Development Center

RADC is the principal AFSC organization charged with planning and executing the USAF exploratory and advanced development programs for information sciences, intelligence, command, control and communications technology, products and services oriented to the needs of the USAF. Primary RADC mission areas are communications, electromagnetic guidance and control, surveillance of ground and aerospace objects, intelligence data collection and handling, information system technology, and electronic reliability, maintainability and compatibility. RADC has mission responsibility as assigned by AFSC for demonstration and acquisition of selected subsystems and systems in the intelligence, mapping, charting, command, control and communications areas.

AMERICAN REVOLUTION BICENTENNIAL
1776-1976